

2. Comparison of the macroscopic properties of $R_2\text{PdSi}_3$ ($R = \text{Gd, Tb, Dy, Ho, Er, Tm}$)

In the introduction some properties of the $R_2\text{PdSi}_3$ ($R = \text{heavy rare earth}$) for which the series caused some interest have been named. The series of $R_2\text{PdSi}_3$ ($R = \text{heavy rare earth}$) has been found to be isostructural with the crystallographic structure described in the introduction (in the $P6/mmm$ space group) [Szytula1999].

Measurements of macroscopic magnetic properties on single crystals had been made for Gd_2PdSi_3 [Mallik1999, Saha1999, Saha2000_2], Tb_2PdSi_3 [Majumdar2000, Paulose2003], Dy_2PdSi_3 [Majumdar2001], Ho_2PdSi_3 [Sampathkumaran2002] and Er_2PdSi_3 [Iyer2005]. Summarizing, the anisotropy in the magnetic properties and the occurrence of multiple metamagnetic transitions had generated interest. Especially, the spin-glass like phase transitions found in Tb_2PdSi_3 and Er_2PdSi_3 [Paulose2003, Iyer2005] have been remarked as unusual. Citing the conclusion of Paulose et al.: “These results clearly reveal that this compound is an exotic magnetic material” [Paulose2003].

The systematic, if present, of the observed effects through the series, had not been investigated. For instance, the role of the crystal-electric field and the exchange interaction had not been separated. This chapter compares macroscopic magnetic properties of different $R_2\text{PdSi}_3$ in the paramagnetic and the ordered state. The role of the different rare earth ions is evaluated. The here presented data have partially been published [Frontzek2006].

2.1 Inverse ac-susceptibilities

Figures 2.1 to 2.6 show the real part of the zero field ac-susceptibility measurements for $R_2\text{PdSi}_3$ with $R = \text{Gd, Tb, Dy, Ho, Er}$ and Tm in the low temperature region. Both directions in-plane ($H, 0, 0$) and perpendicular to the basal plane ($0, 0, L$) (in the following addressed as crystallographic \mathbf{a} - and \mathbf{c} -direction) are shown. The \mathbf{a} -direction is depicted with a grey color while the \mathbf{c} -direction is shown in black. In figure 2.1, the left and right y-axis of the graph has the identical scale. In the other graphs the scale is adjusted to ideally display the zero field ac-susceptibility of both the \mathbf{a} - and \mathbf{c} -direction. The scale differs up to two orders of magnitude (in the case of Tb_2PdSi_3). Tm_2PdSi_3 has been measured in an inhomogeneous ac-field in a complete different ac-susceptibility setup since the normally employed ac-susceptometer allows temperatures only down to 2 K. Due to this neither a comparison of the value nor the magnitude of both curves is possible.

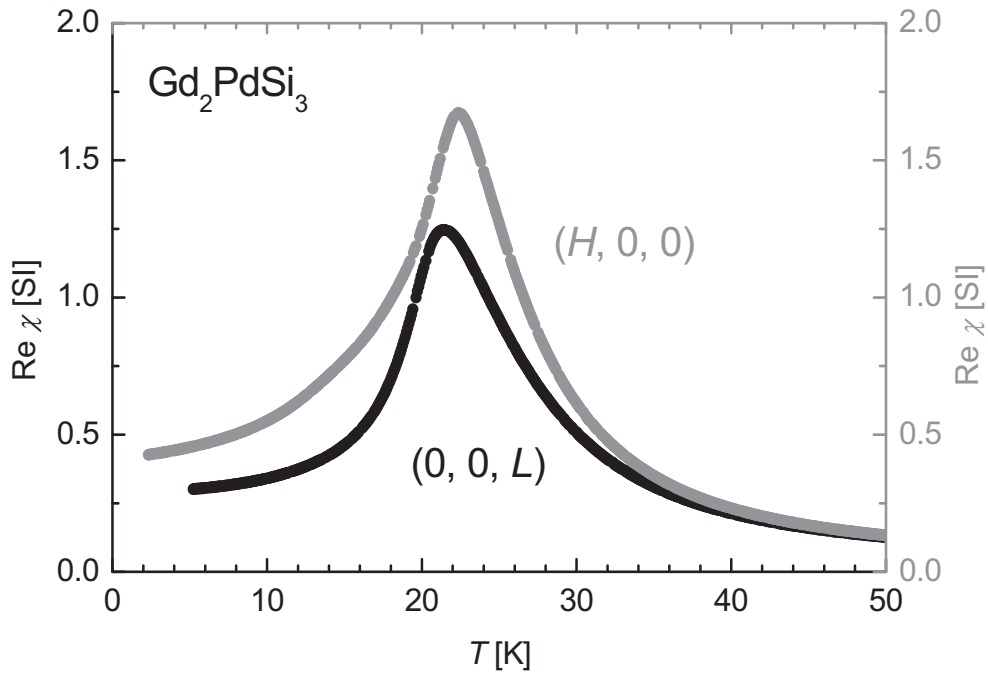


Figure 2.1: Real part of the zero field ac-susceptibility of single crystalline Gd_2PdSi_3 . The measurement with the ac-field along $(0, 0, L)$ and $(H, 0, 0)$ are shown in black and grey, respectively.

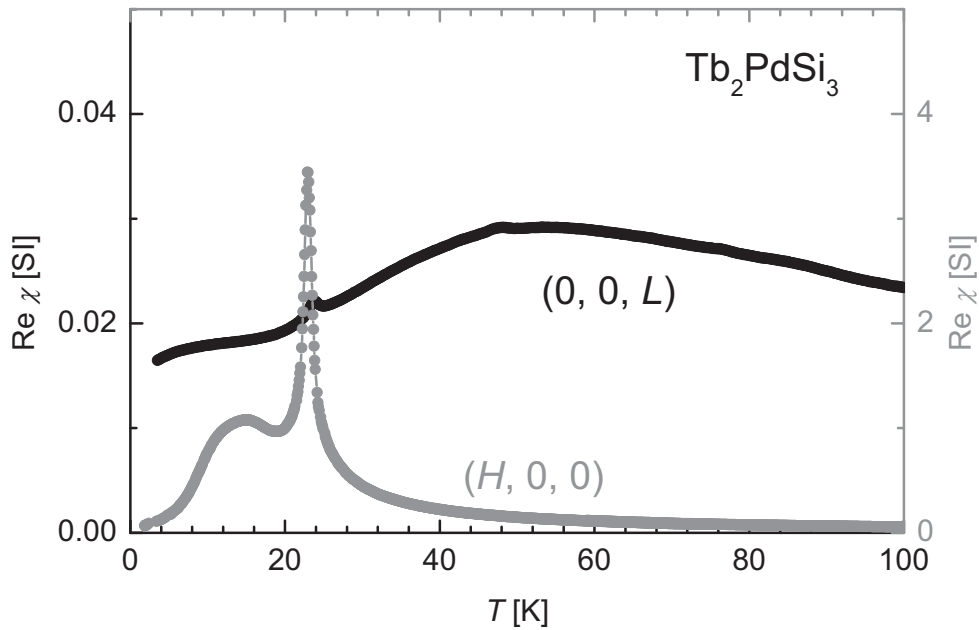


Figure 2.2: Real part of the zero field ac-susceptibility of single crystalline Tb_2PdSi_3 . The measurement with the ac-field along $(0, 0, L)$ and $(H, 0, 0)$ are shown in black and grey, respectively. Mind the different values of the susceptibility (left and right y-axis).

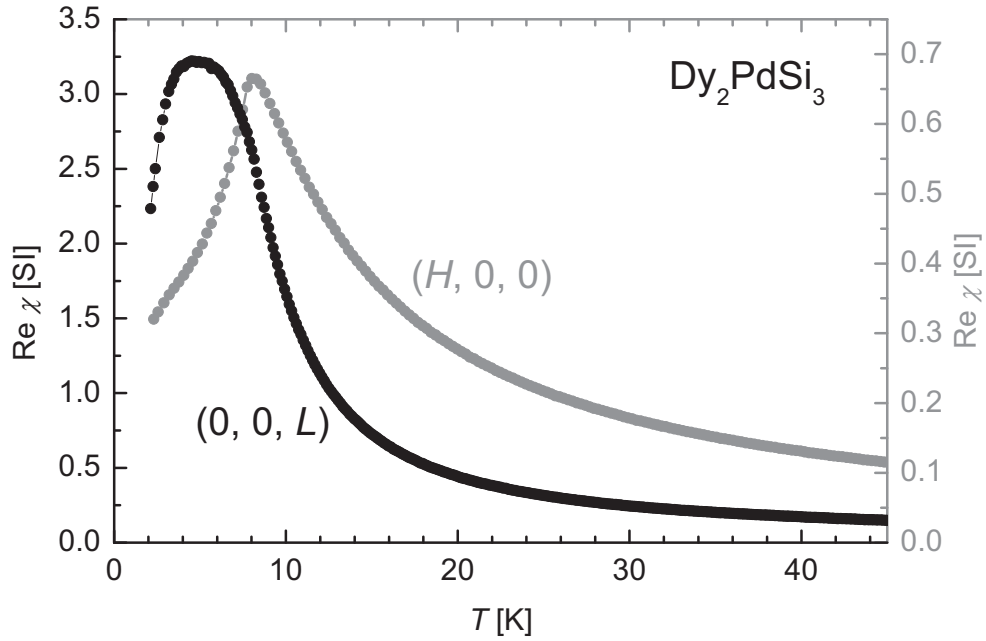


Figure 2.3: Real part of the zero field ac-susceptibility of single crystalline Dy_2PdSi_3 . The measurement with the ac-field along $(0, 0, L)$ and $(H, 0, 0)$ are shown in black and grey, respectively. Mind the different values of the susceptibility (left and right y-axis).

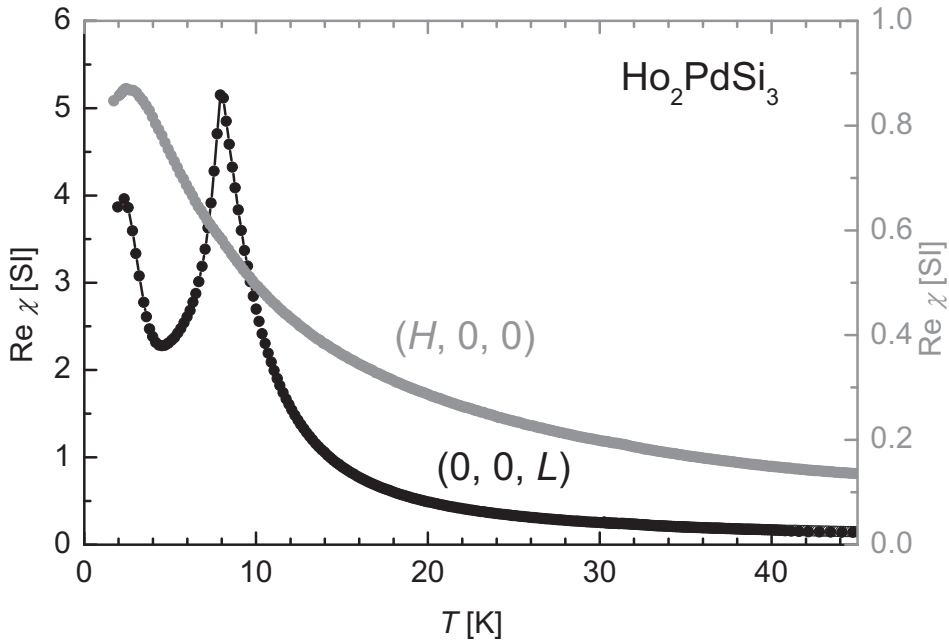


Figure 2.4: Real part of the zero field ac-susceptibility of single crystalline Ho_2PdSi_3 . The measurement with the ac-field along $(0, 0, L)$ and $(H, 0, 0)$ are shown in black and grey, respectively. Mind the different values of the susceptibility (left and right y-axis).

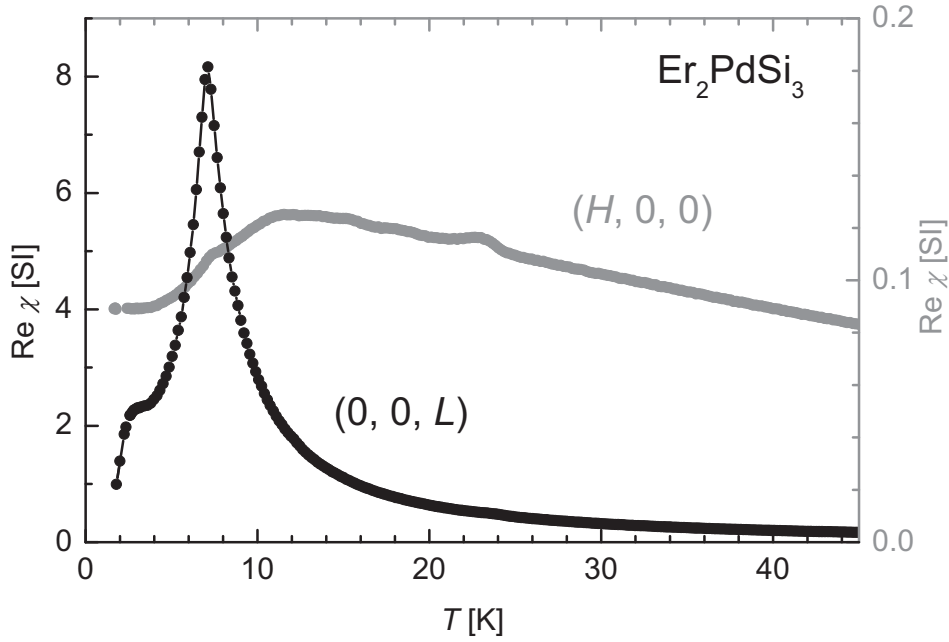


Figure 2.5: Real part of the zero field ac-susceptibility of single crystalline Er_2PdSi_3 . The measurement with the ac-field along $(0, 0, L)$ and $(H, 0, 0)$ are shown in black and grey, respectively. Mind the different values of the susceptibility (left and right y -axis).

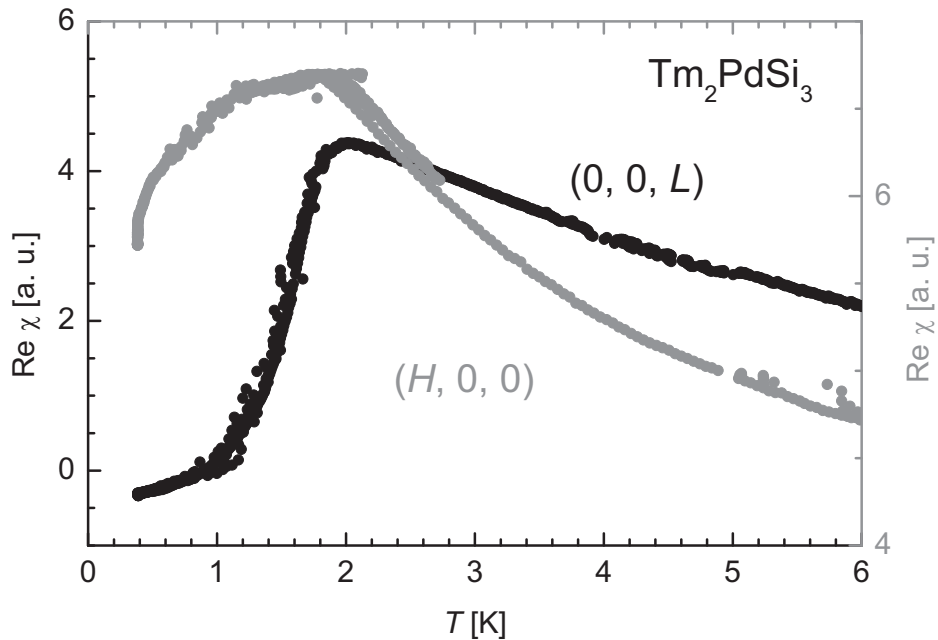


Figure 2.6: Real part of the zero field ac-susceptibility of single crystalline Tm_2PdSi_3 . The measurement with the ac-field along $(0, 0, L)$ and $(H, 0, 0)$ are shown in black and grey, respectively. The values of the susceptibility are arbitrary (also relative to each axis) due to the special measurement setup.

2. Comparison of the macroscopic properties of $R_2\text{PdSi}_3$ ($R = \text{Gd}, \text{Tb}, \text{Dy}, \text{Ho}, \text{Er}, \text{Tm}$)

The comparison of the value of the ac-susceptibility for both measured directions defines the easy (hard) magnetic axis of the compound. In the following the magnetic hard (easy) direction is defined by the low (high) values of the susceptibility in the paramagnetic state.

From the positions of the absolute maxima of the respective easy magnetic axis the ordering temperatures T_N have been determined and are listed in Table 1.

R	T_N [K]	$(g_J-1)^2 \cdot J(J+1)$	$\mu_{\text{eff}} [\mu_B]$	$\mu_{\text{th}} [\mu_B]$	θ_c [K]	θ_a [K]	$\alpha \cdot 10^2$
Gd	22.3	15.75	8.0±0.2	7.937	30.3±0.7	30.7±1.2	-
Tb	23.6	10.5	9.6±0.3	9.72	-32.5±1.4	24.0±1.4	-1.0101
Dy	8.2	7.083	10.3±0.3	10.65	-1.4±1.4	11.5±1.4	-0.6349
Ho	7.7	4.5	10.2±0.3*	10.61	-	4.3±1.4*	-0.2222
Er	7.0	2.55	9.4±0.2	9.58	15.2±1.1	-7.5±1.1	0.2540
Tm	1.8	1.2	7.5±0.2	7.56	19.1±0.6	-15.6±0.6	0.10101

Table 1: Compilation of results of the Curie-Weiss analysis for $R_2\text{PdSi}_3$ and theoretical values for R^{3+} ions:
- T_N Néel temperature determined from experiments;
- $(g_J-1)^2 J(J+1)$ DeGennes factor;
- μ_{eff} effective paramagnetic moment from the Curie-Weiss analysis.
- μ_{th} theoretical value according to Hund's rule;
- θ_c and θ_a asymptotic paramagnetic Curie temperatures from the Curie-Weiss analysis for the measurements parallel c and a , respectively;
- α Stevens parameter from reference [Hutchings1964]
* For Ho_2PdSi_3 only the values for the a -axis are considered (see text);

Below T_N the c -axis is the easy magnetic axis for the compounds with $R = \text{Dy}, \text{Ho}$ and Er while it is the magnetic hard axis for $R = \text{Gd}$ and Tb . The magnetic easy axis of Tm_2PdSi_3 cannot be determined from the special ac-susceptibility setup. The compounds with $R = \text{Dy}, \text{Ho}$ and Er order at $T_N = 8.2$ K, 7.7 K and 7.0 K, respectively, while the Tb compound has the highest ordering temperature of the whole series with $T_N = 23.6$ K. These temperatures are in agreement with the previously reported values from powder measurements [Szytula1999, Kotsanidis1990]. Interestingly, the ordering temperatures of the series do not obey a DeGennes scaling law [DeGennes1962]. Figure 2.7 shows the comparison of the ordering temperatures and the DeGennes factor for the different $R_2\text{PdSi}_3$ compounds. Four compounds show an additional anomaly below T_N in the investigated temperature range which probably corresponds to a second phase transition. These four compounds are Tb_2PdSi_3 , Ho_2PdSi_3 , Dy_2PdSi_3 and Er_2PdSi_3 . In Tb_2PdSi_3 the broad maximum at about 10 K has been connected to a spin-glass like transition [Paulose2003]. The additional anomaly in Ho_2PdSi_3 , a maximum observed for both easy and hard axis, is found around 2 K. In Dy_2PdSi_3 a kink is observed in

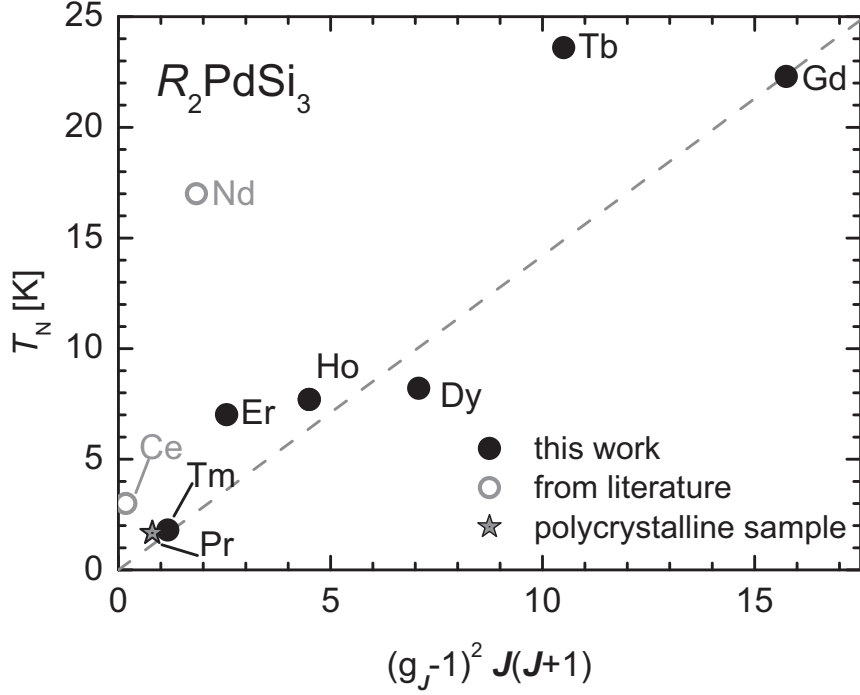


Figure 2.7: Ordering temperatures of $R_2\text{PdSi}_3$ (T_C in the case of Nd) compounds vs. the DeGennes factor. The literature values are from reference [Szytula1999].

the easy direction while in the hard direction a strong reduction of the signal is found around 2 K. For Er_2PdSi_3 the anomaly has been attributed to a spin-glass like transition at $T = 2$ K [Iyer2005].

Figures 2.8 to 2.13 show the inverse ac susceptibility vs. temperature for $R_2\text{PdSi}_3$ ($R = \text{Gd, Tb, Dy, Ho, Er, Tm}$). At high temperatures the susceptibility is described by a Curie-Weiss law:

$$\chi = \frac{C}{T - \theta_p} \quad (12)$$

The light grey lines represent a Curie-Weiss fit used to yield the asymptotic paramagnetic Curie temperatures θ_p for each crystallographic direction (in the following labeled θ_a and θ_c for the asymptotic-paramagnetic Curie temperature in the crystallographic a - and c -direction, respectively). The antiferromagnetic transition temperatures determined from the maximum of the ac-susceptibility curves (see figure 2.1 to 2.6) are marked by an arrow in Figs. 2.8 to 2.13.

The inverse zero-field ac-susceptibilities up to 300 K for the crystallographic a - and c -direction on Gd_2PdSi_3 are shown in figure 2.8. The paramagnetic properties of Gd_2PdSi_3 above the ordering temperature of 22 K are isotropic within the experimental variance. This is expected since Gd^{3+} is an S -state ion and is not susceptible to the crystal electric field effect.

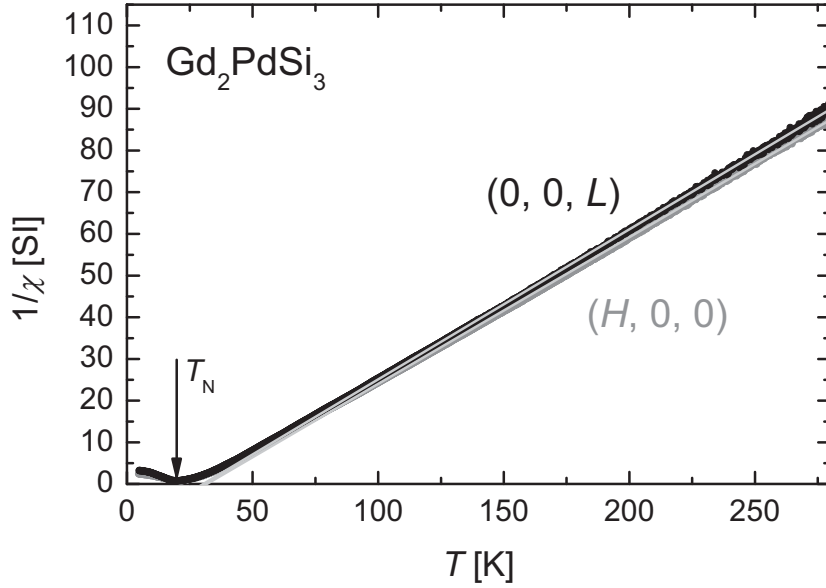


Figure 2.8: Inverse Gd_2PdSi_3 single crystal ac-susceptibility data along the $(0, 0, L)$ and $(H, 0, 0)$ direction. The Néel temperature is marked. The light grey lines are the Curie Weiss fit (see text).

Roughly above 55 K the course of the inverse susceptibility can be effectively described by a Curie-Weiss behavior. The effective paramagnetic moment is $\mu_{\text{eff}} = 8.0 \mu_{\text{B}}$ in excellent agreement with the expected value of $\mu_{\text{th}} = 7.937 \mu_{\text{B}}$ [Hund1925]. The asymptotic paramagnetic Curie temperature is around +30 K. The surprisingly large positive value of θ_{p} indicates ferromagnetic correlations of the antiferromagnetically ordering compound. The values of the effective paramagnetic moment and the asymptotic paramagnetic Curie temperatures are summarized in table 1.

In the case of Er_2PdSi_3 (Fig. 2.9) the magnetic hard axis is the \mathbf{a} -axis and the magnetic easy axis is the hexagonal \mathbf{c} axis. This behavior is associated with a prolate shape of the $4f$ -charge distribution of the trivalent Er^{3+} ion with a positive Stevens factor $\alpha > 0$ (see table 1). Above 50 K (corresponding to seven times T_{N}) paramagnetic behavior according to the Curie-Weiss law is found for both axes (fit from 50 K to 250 K). The anisotropy between magnetic hard and easy axis is well pronounced, yielding a small negative θ_{a} and a larger positive θ_{c} (see table 1). The slopes of both inverse susceptibility curves are equal resulting in an experimental paramagnetic moment of $\mu_{\text{eff}} = 9.4 \mu_{\text{B}}$ in good agreement with the theoretical free-ion value for Er^{3+} ($\mu_{\text{th}} = 9.58 \mu_{\text{B}}$).

In contrast to Er_2PdSi_3 one observes for the Tb_2PdSi_3 compound (Fig. 2.10) that the magnetic easy axis is the in-plane \mathbf{a} -axis and the magnetic hard axis is the hexagonal \mathbf{c} -axis. The interchange of magnetic easy and hard axis corresponds to the opposite sign of the Stevens factor α of Tb^{3+} ($\alpha < 0$) in comparison to Er^{3+} . The anisotropy found for the Tb_2PdSi_3

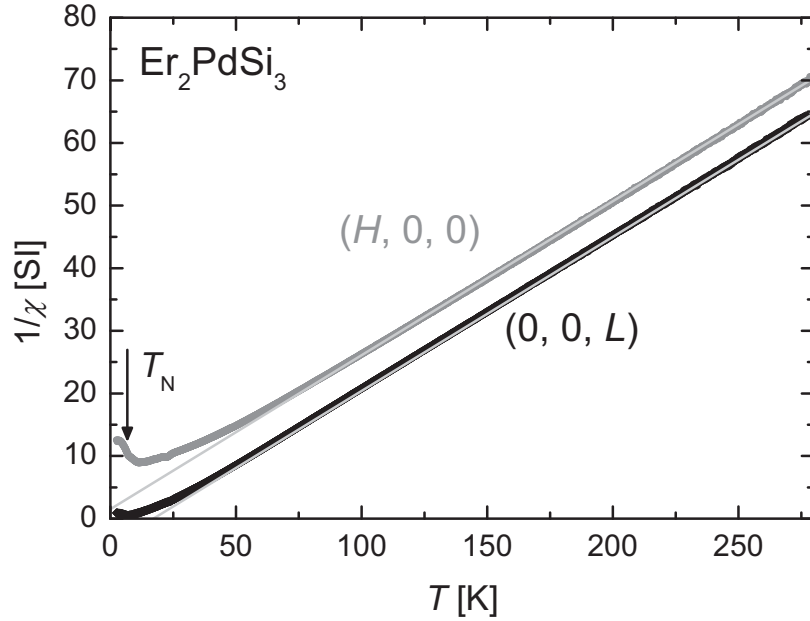


Figure 2.9: Inverse Er_2PdSi_3 single crystal ac-susceptibility data along the $(0, 0, L)$ and $(H, 0, 0)$ direction. The Néel temperature is marked.

compound is even more pronounced than for the Er_2PdSi_3 compound. One observes for the magnetic easy axis paramagnetic Curie-Weiss behavior right above the ordering temperature of 23.6 K while a deviation from the Curie-Weiss law is observed in the magnetic hard direction up to 100 K (4 times T_N). For temperatures above 100 K the slopes of the inverse susceptibility curves for both directions are equal. The paramagnetic moment from the Curie-

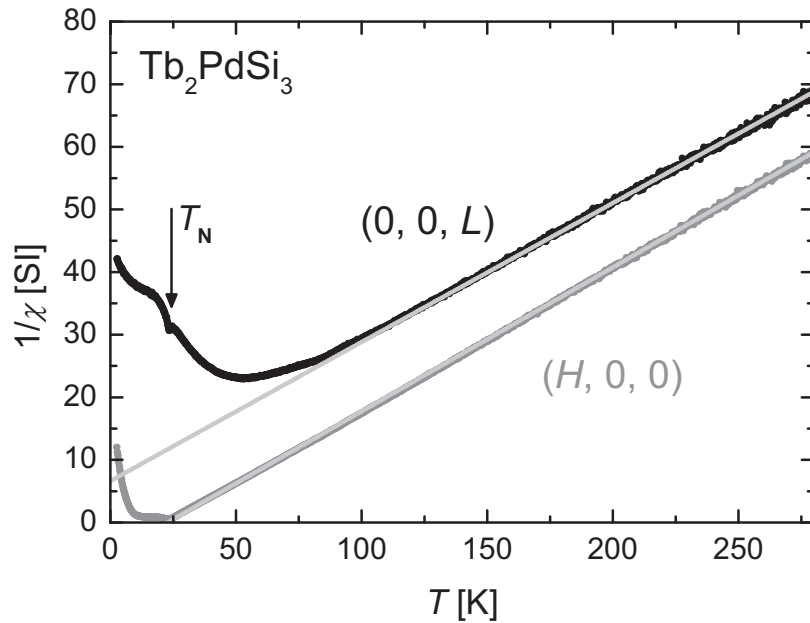


Figure 2.10: Inverse Tb_2PdSi_3 single crystal ac-susceptibility data along the $(0, 0, L)$ and $(H, 0, 0)$ direction. The Néel temperature is marked.

Weiss fit is $\mu_{\text{eff}} = 9.68 \mu_{\text{B}}$ in good agreement with the free-ion value of Tb^{3+} ($\mu_{\text{th}} = 9.72 \mu_{\text{B}}$). The asymptotic paramagnetic Curie temperature is positive for the a -direction and negative for the c -direction.

The anisotropic $4f$ -charge distribution of the rare earth ions Dy^{3+} and Ho^{3+} (both having $\alpha < 0$) is expected to produce the same anisotropy as for the Tb_2PdSi_3 compound although less pronounced because of the smaller values for α . In the case of Dy_2PdSi_3 (figure 2.11) the expected anisotropy as well as the Curie-Weiss behavior is found for temperatures above 70 K (9 times T_{N}). The observed anisotropy for Dy_2PdSi_3 is smaller than for Er_2PdSi_3 though the magnitude of α is larger. The analysis of the linear behavior yields an effective magnetic moment of $\mu_{\text{eff}} = 10.3 \mu_{\text{B}}$ which is insignificantly smaller than the free-ion value for Dy^{3+} ($\mu_{\text{th}} = 10.64 \mu_{\text{B}}$). The behavior is characterized by a positive asymptotic paramagnetic Curie

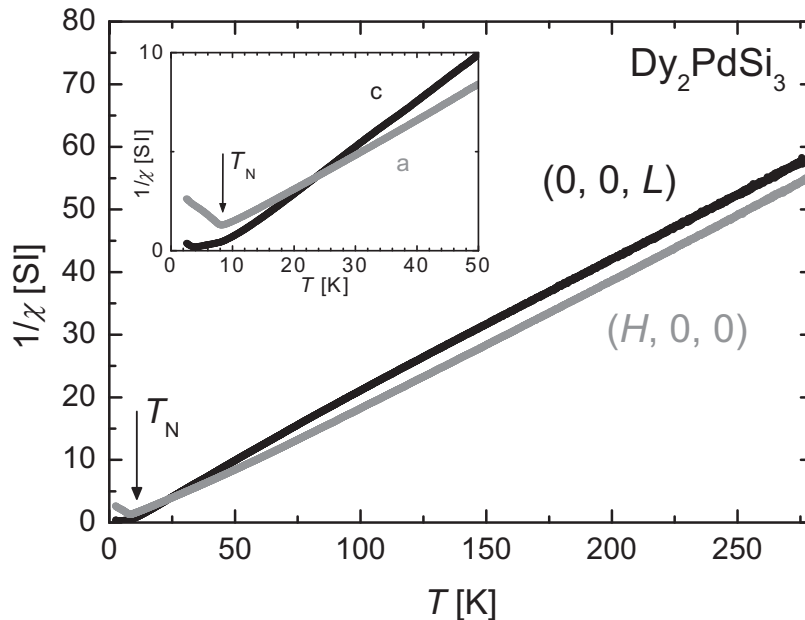


Figure 2.11: Inverse Dy_2PdSi_3 single crystal ac-susceptibility data along the $(0, 0, L)$ and $(H, 0, 0)$ direction. The Néel temperature is marked.

temperature for the a -direction while the Curie temperature for the c -direction is negative but close to zero. Below 70 K a deviation from the Curie-Weiss behavior is observed leading to a crossing point at around 25 K, well above the ordering temperature of $T_{\text{N}} = 8.2$ K. Below 25 K the a -axis is the magnetic hard axis while the c axis has become the magnetic easy axis.

From the magnitude of α , Ho_2PdSi_3 (fig. 2.12) is expected to show a small anisotropy. In figure 2.12 the inverse susceptibility curves have different slopes for the two crystallographic directions. This unusual behavior yields $\mu_{\text{eff}} = 10.2 \mu_{\text{B}}$ and $9.6 \mu_{\text{B}}$ for the a - and c -direction, respectively. The value for the c -direction is significantly lower than the free ion value for

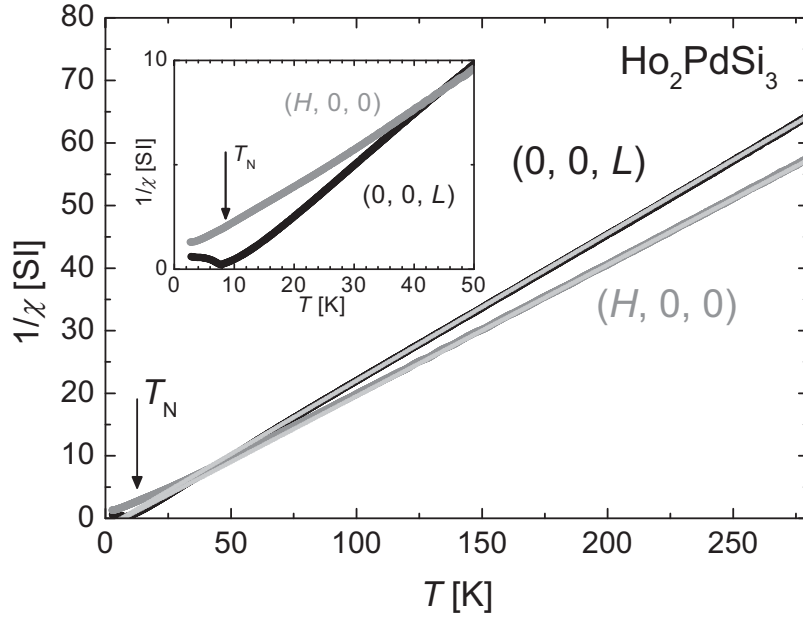


Figure 2.12: Inverse Ho_2PdSi_3 single crystal ac-susceptibility data along the $(0, 0, L)$ and $(H, 0, 0)$ direction. The Néel temperature is marked.

Ho^{3+} ($\mu_{\text{th}} = 10.61 \mu_{\text{B}}$) while the value for the \mathbf{a} -direction is only slightly below that value. Therefore, for μ_{eff} of Ho_2PdSi_3 we have only used the latter value (see table 1). In addition, no value for θ_{c} is listed in Table 1. In the high temperature regime the \mathbf{a} -axis is the magnetic easy axis as one would expect from the negative sign of the Stevens factor. At a temperature of about 40 K one observes a crossing of the inverse susceptibilities. Below 40 K the \mathbf{a} -axis becomes the magnetic hard axis while the \mathbf{c} axis becomes the magnetic easy axis.

Tm_2PdSi_3 (fig. 2.13 on the next page) undergoes a magnetic transition around 1.8 K. This transition was confirmed by an additional specific heat measurement (see inset of fig. 2.13). The magnitude of the Stevens factor α for the Tm^{3+} ion is the same as for the Tb^{3+} ion but with opposite sign. Therefore, the anisotropy is similarly pronounced as in the case of the Tb_2PdSi_3 compound. Because of the opposite sign of the Stevens factor the \mathbf{a} -axis is the magnetic hard axis and the \mathbf{c} axis is the magnetic easy direction as in the Er_2PdSi_3 compound. Above a temperature of 80 K for the easy \mathbf{c} axis and above 25 K for the hard \mathbf{a} -axis the susceptibility is in accordance to a Curie-Weiss law. Interestingly, in the other investigated compounds the temperatures for which deviation from a Curie-Weiss behavior is observed are lower for the easy and higher for the hard direction in contrast to Tm_2PdSi_3 . The Curie-Weiss fit yields an effective moment of $\mu_{\text{eff}} = 7.5 \mu_{\text{B}}$ which agrees well with the expected value for Tm^{3+} ($\mu_{\text{th}} = 7.58 \mu_{\text{B}}$).